

1 **Effect of temperature on the formation of highly oxygenated organic**
2 **molecules (HOM) from alpha-pinene ozonolysis**

3
4 **Lauriane L. J. QUÉLÉVER**¹, Kasper KRISTENSEN^{2*}, Louise NORMANN JENSEN², Bernadette
5 ROSATI^{2,3}, Ricky TEIWES^{2,3}, Kaspar R. DAELLENBACH¹, Otso PERÄKYLÄ¹, Pontus ROLDIN⁴,
6 Rossana BOSSI⁵, Henrik B. PEDERSEN³, Marianne GLASIUS², Merete BILDE², and Mikael EHN¹.

7
8 ¹ Institute for Atmospheric and Earth System Research – INAR / Physics, P.O. Box 64, FI-00014 University
9 of Helsinki, Finland.

10 ² Aarhus University, Department of Chemistry, Langelandsgade 140, DK-8000 Aarhus C, Denmark.

11 ³ Aarhus University, Department of Physics and Astronomy, Ny Munkegade 120, DK-8000 Aarhus C,
12 Denmark.

13 ⁴ Lund University, Division of Nuclear Physics, P.O. Box 118, SE-22100 Lund, Sweden.

14 ⁵ Aarhus University, Department of Environmental Science, Frederiksborgvej 399, DK-4000 Roskilde,
15 Denmark.

16 * Presently at Aarhus University, Department of Engineering, Finlandsgade 12, DK-8200 Aarhus N, Denmark.

17
18 *Correspondence to* Lauriane QUÉLÉVER (Lauriane.quelever@helsinki.fi) & Mikael EHN

19 (Mikael.ehn@helsinki.fi)

20

21

22 **Abstract**

23

24 Highly-oxygenated organic molecules (HOM) are important contributors to Secondary Organic Aerosol
25 (SOA) and New-Particle Formation (NPF) in the boreal atmosphere. This newly discovered class of molecules
26 is efficiently formed from atmospheric oxidation of biogenic volatile organic compounds (VOC), such as
27 monoterpenes, through a process called autoxidation. This process, in which peroxy-radical intermediates
28 isomerize to allow addition of molecular oxygen, is expected to be highly temperature-dependent. Here, we
29 studied the dynamics of HOM formation during α -pinene ozonolysis experiments performed at three different
30 temperatures, 20 °C, 0 °C and -15 °C, in the Aarhus University Research on Aerosol (AURA) chamber. We
31 found that the HOM formation, under our experimental conditions (50 ppb α -pinene, 100 ppb ozone),
32 decreased considerably as temperature decreased, with molar yields dropping by around a factor of 50 when
33 experiments were performed at 0 °C, compared to 20 °C. At -15 °C, the HOM signals were already close to
34 the detection limit of the nitrate-based Chemical Ionization Atmospheric Pressure interface Time Of Flight
35 (CI-APi-TOF) mass spectrometer used for measuring gas-phase HOM. Surprisingly, comparing spectra
36 measured at 0 °C and 20 °C, ratios between HOM of different oxidation level, e.g. the typical HOM products
37 $C_{10}H_{14}O_7$, $C_{10}H_{14}O_9$, and $C_{10}H_{14}O_{11}$, changed considerably less than the total HOM yields. The more oxidized
38 species have undergone more isomerization steps, yet, at lower temperature, they did not decrease more than
39 the less oxidized species. One possible explanation is that the primary rate-limiting step forming these HOM
40 occurs before the products become oxygenated enough to be detected by our CI-APi-TOF (i.e. typically seven
41 or more oxygen atoms). The strong temperature dependence of HOM formation was observed under
42 temperatures highly relevant for the boreal forest, but the exact magnitude of this effect in the atmosphere will
43 be much more complex: the fate of peroxy-radicals is a competition between autoxidation (influenced by
44 temperature and VOC type) and bimolecular termination pathways (influenced mainly by concentration of
45 reaction partners). While the temperature influence is likely smaller in the boreal atmosphere than in our
46 chamber, the magnitude and complexity of this effect clearly deserves more consideration in future studies in
47 order to estimate the ultimate role of HOM on SOA and NPF under different atmospheric conditions.

48

49 **Keywords:** HOM formation & yield, Temperature, ACCHA campaign, AURA chamber, Mass Spectrometry,
50 CI-APi-TOF

51

52 **1. Introduction**

53

54 Aerosol particles impact Earth's climate by scattering and absorbing solar radiation, and by influencing cloud
55 properties when they act as Cloud Condensation Nuclei (CCN) (IPCC, 2013). Organic compounds contribute
56 significantly to the chemical composition of aerosol, accounting from 20 % to 90 % of the total aerosol mass
57 of sub-micrometer particles depending on their location in the globe (Jimenez et al., 2009). Submicron organic
58 aerosol are dominantly secondary. Called Secondary Organic Aerosol (SOA), they originate from gas-to-
59 particle conversion from condensable vapors (Hallquist et al., 2009; Zhang et al., 2007). These vapors are
60 mainly oxidation products of Volatile Organic Compounds (VOC), having sufficiently low vapor pressure (i.e.
61 volatility) to condense onto aerosol particles (Hallquist et al., 2009).

62

63 In order to interact efficiently with solar radiation or to activate cloud droplets, aerosol particles need to be
64 around 100 nm in diameter or larger (Dusek et al., 2006). If particles have formed through nucleation processes
65 in the atmosphere (e.g. Kulmala et al., 2013), their ability to grow to climate-relevant sizes before being
66 scavenged through coagulation is critically impacted by the rate at which low-volatile vapors will condense
67 onto them (Donahue et al., 2013). Extremely Low-Volatile Organic Compounds (ELVOC), introduced by
68 Donahue et al. (2012), have the ability to condense irreversibly onto even the smallest aerosol particles and
69 clusters and thus contribute to particle growth. Low-Volatile Organic Compounds (LVOC), typically more
70 abundant in the atmosphere, are important for the growth of particles larger than a few nanometers (Tröstl et
71 al., 2016).

72

73 Highly-oxygenated Organic Molecules (HOM, Ehn et al., 2014 & 2017; Bianchi et al., 2019) were recently
74 identified as a large contributor to (E)LVOC and the growth of newly formed particles (Ehn et al., 2014; Tröstl
75 et al., 2016). First observed in measurements of naturally charged ions in the boreal forest (Ehn et al., 2010 &

76 2012) using the Atmospheric Pressure interface Time Of Flight (APi-TOF) mass spectrometer (Junninen et
77 al., 2010), HOM quantification only became possible through the application of nitrate ion chemical ionization
78 (CI) mass spectrometry (Zhao et al., 2013; Ehn et al., 2014). Most studies have utilized the APi-TOF coupled
79 to such a chemical ionization source (CI-APi-TOF, Jokinen et al., 2012), and detailed laboratory studies have
80 been able to elucidate the primary formation pathways of HOM (Rissanen et al., 2014; Jokinen et al., 2014;
81 Mentel et al., 2015). We also note that the HOM-related terminology has evolved over the last years, and here
82 we define HOM as organic molecules formed through gas-phase autoxidation, containing six or more oxygen
83 atoms.

84

85 The main process in HOM formation is peroxy-radical (RO₂) autoxidation (Crouse et al., 2013), which
86 involves an intramolecular H-abstraction by the peroxy-radical group to form a hydroperoxide and a carbon-
87 centered radical to which molecular oxygen (O₂) can rapidly add to form a new RO₂ with a higher level of
88 oxygenation. The efficiency of this process is mainly determined by the availability of easily “abstractable”
89 H-atoms, and such are often formed in the ozonolysis of endocyclic alkenes (Rissanen et al., 2014 & 2015;
90 Berndt et al., 2015). This structural component can be found in many biogenic VOC, such as monoterpenes,
91 enhancing their roles as SOA precursors through efficient autoxidation and HOM formation (Ehn et al., 2014;
92 Jokinen et al., 2014; Berndt et al., 2016). Peroxy-radicals are important intermediates in nearly all atmospheric
93 oxidation processes. The RO₂ that have undergone autoxidation will terminate to closed-shell species in similar
94 ways as less oxidized RO₂, taking place either by unimolecular processes leading to loss of OH or HO₂, or
95 bimolecular reactions with NO, HO₂ or other RO₂. The termination pathway strongly influences the type of
96 HOM that can be formed, with e.g. RO₂ + RO₂ reactions being able to form ROOR dimers and RO₂+NO often
97 forming organic nitrates (Ehn et al., 2014; Berndt et al., 2018). All these bimolecular reactions of peroxy-
98 radicals, as well as the initial oxidant-VOC reaction, are temperature-dependent. For example, the reaction rate
99 of ozone with α -pinene, a broadly studied SOA-forming system, is $6.2 \cdot 10^{17} (\pm 1.3 \cdot 10^{17}) \text{ cm}^3 \text{ molec}^{-1} \text{ s}^{-1}$ at 3
100 °C, and $8.3 \cdot 10^{17} (\pm 1.3 \cdot 10^{17}) \text{ cm}^3 \text{ molec}^{-1} \text{ s}^{-1}$ at 22 °C (Atkinson et al., 1982). However, the intramolecular
101 isomerization through H-shifts is likely to have a much stronger temperature dependence, due to the higher
102 energy barrier for the H-shift (Seinfeld and Pandis, 2006; Otkjær et al., 2018). As an example (Praske et al.,
103 2018) reported theoretical estimates of different H-shifts in hexane-derived RO₂ which increased roughly by

104 a factor of 5 to 10 when the temperature increases by 22 °C (from 23 °C to 45 °C). Possible changes in HOM
105 formation as a function of temperature are thus expected to derive mainly from changes in the autoxidation
106 process. However, a detailed mechanistic understanding the various autoxidation steps, let alone their
107 temperature dependencies, is still lacking for most atmospheric VOC-oxidant systems, owing partly to the
108 plethora and the complexity of the possible reaction pathways.

109

110 Despite recent work in determining the impact of temperature on aerosol formation (Kristensen et al., 2017;
111 Stolzenburg et al., 2018), literature on corresponding HOM effects are extremely limited. At room temperature
112 (i.e. 20 ± 5 °C), HOM molar yields have been estimated to be some percent for most monoterpenes in reactions
113 with ozone or OH (Ehn et al., 2014; Jokinen et al., 2015). Only very recently, studies were presented where
114 HOM formation experiments have been conducted at varying temperatures. Stolzenburg et al. (2018) showed
115 that at lower temperatures, the CI-APi-TOF detects much lower HOM concentrations, though no quantitative
116 values on the HOM yields were given. The impact of decreased HOM on new-particle growth rates was
117 compensated by less oxidized species being able to condense at the lower temperatures. In another study, Frege
118 et al. (2018) also concluded that HOM formation decreased at lower temperatures, but their study was based
119 on observations of naturally charged ions using an APi-TOF, complicating the interpretation of HOM
120 formation rates.

121

122 In this study, we directly evaluate the impact of temperature on HOM yields in a laboratory chamber during
123 α -pinene ozonolysis experiments at 20 °C, 0 °C and -15 °C. Relative changes in HOM formation are compared
124 between temperatures both for total HOM yields as well as on a molecule-by-molecule basis. The more
125 detailed impact of temperature on the molecular distribution of HOM is expected to provide new insights into
126 critical steps in the formation pathways.

127

128

129 **2. Methods**

130

131 **2.1. The AURA Chamber**

132 A detailed description of the AURA chamber can be found in Kristensen et al. (2017). Essentially, it consists
133 of a 5 m³ Teflon® bag contained in a temperature-controlled enclosure. Configured in batch sampling mode,
134 the chamber was initially cleaned by flushing at 20 °C with purified ambient air (i.e. filtered air exempt of
135 particles, water vapor and VOC, and reduced NO_x concentration), and subsequently set to the desired
136 temperature and finally filled with the necessary reagents. Over the course of the experiment, it was
137 progressively emptied due to sampling by the measuring instrumentation. In our experiments, we first added
138 ozone to a concentration of 100 ppb, provided by an ozone generator (Model 610, Jelight Company, Inc.) after
139 which the oxidation reaction started when the VOC was introduced by vaporization of a calculated volume of
140 liquid reagent (α -pinene or β -pinene) into a hot stream of nitrogen, reaching the desired VOC concentration
141 (10 or 50 ppb).

142

143 **2.2. The ACCHA Experiment**

144 The Aarhus Chamber Campaign on HOM and Aerosols (ACCHA) experiment aimed to explore oxidation
145 processes and aerosol formation during dark monoterpene ozonolysis at different temperatures, from -15 °C
146 to 20 °C. The experiments focused on α -pinene oxidation at two different concentrations (10 ppb and 50 ppb)
147 for three different temperatures: -15 °C, 0 °C and 20 °C. Two additional experiments were conducted with
148 temperatures ramped from the coldest to the warmest or reversely during experiments at 10 ppb of α -pinene.
149 For comparison, fixed temperature runs were also performed using β -pinene, at a concentration of 50 ppb.
150 Ozone (100 ppb) was used as the main oxidant, but hydroxyl radicals also took part in the oxidation reactions
151 as OH-scavengers were not employed in the experiments discussed here. According to model simulations using
152 the master chemical mechanism v3.3.1 (Jenkin et al., 1997 & 2015; Saunders et al., 2003), ozonolysis
153 accounted for approximately 2/3 and OH-oxidation for 1/3 of the α -pinene oxidation respectively. A table
154 summarizing the experiments of the campaign can be found in the Appendix (Table A1).

155

156 **2.3. Instrumentation**

157 The ACCHA experiment involved a diverse set of instruments measuring both the gas phase and the particle
158 phase. The gas phase instrumentation included a Proton Transfer Reaction Time Of Flight Mass Spectrometer
159 (PTR-TOF-MS, Model 8000-783, IONICON Inc., Jordan et al., 2009) for measuring the concentrations of the
160 injected VOCs and other volatile products, as well as a nitrate-based Chemical Ionization Atmospheric
161 Pressure interface Time of Flight (CI-APi-TOF, TOFWERK A.G. & Aerodyne Research Inc., Jokinen et al.,
162 2012) mass spectrometer, analyzing the highly oxidized organic products of lower volatility (e.g. HOM). The
163 CI-APi-TOF is described in more detail in the following section. The aerosol phase measurement was done
164 using (1) a nano-Condensation Nuclei Counter (nCNC), being a combination of a Particle Size Magnifier
165 (PSM, Model A10, Airmodus Ltd.) and a Condensation Particle Counter (CPC, Model A20, Airmodus Ltd.),
166 (2) a Scanning Mobility Particle Sizer (SMPS; Kr-85 neutralizer (Model 3077A, TSI), electrostatic classifier
167 (Model 3082, TSI), nano-water-based CPC (Model 3788, TSI)), counting the size resolved particles from 10
168 nm to 400 nm, (3) a High Resolution Time-Of-Flight Aerosol Mass Spectrometer (HR-TOF-AMS, Aerodyne
169 Research Inc., Jayne et al., 2000) determining the chemical composition of non-refractory aerosol particles
170 larger than ~35 nm. The temperature and relative humidity inside the chamber were monitored using HC02-
171 04 sensors (HygroFlex HF320, Rotronic AG), and the ozone concentration was measured with an ozone
172 monitor (O₃-42 Module, Environment S.A.).

173

174 **2.4. Measuring highly oxygenated organic molecules in the gas phase**

175 HOM present in the gas phase were measured using a CI-APi-TOF mass spectrometer. The instrument sampled
176 air at about 80 cm from the wall of the chamber via a $\frac{3}{4}$ inch tube directly connected to the CI-APi-TOF, which
177 was located outside the chamber enclosure (~20 °C at all time). The sheath air (taken from a compressed air
178 line) was 30 LPM and the total flow (generated by the house vacuum line) was 40 LPM. The ~1 m long inlet
179 had a flow of 10 LPM caused by the difference between the sheath and total flows. With such a tube length
180 and flow, roughly half of the HOM are expected to be lost to the walls of the inlet lines. The CI-APi-TOF is
181 described by Jokinen et al. (2012), but also briefly presented here. Strong acids and highly oxygenated organic

182 molecules have been shown to cluster efficiently with nitrate ion (Ehn et al., 2014; Hyttinen et al., 2015).
183 Nitrate ions (i.e. NO_3^- , $\text{HNO}_3\text{NO}_3^-$ and $(\text{HNO}_3)_2\text{NO}_3^-$), produced by exposure of nitric acid vapors to soft X-
184 ray radiation, were electrostatically introduced into the sample flow of 10 LPM with a reaction time of roughly
185 200 ms at atmospheric pressure.

186 The ions, clusters with NO_3^- , were sampled through a 300 μm critical orifice into the APi, where ions were
187 guided and focused by two segmented quadrupoles through chambers with gradually decreasing pressures (~ 2
188 mbar and $\sim 10^{-2}$ mbar, respectively). Finally, an ion lens assembly, at $\sim 10^{-5}$ mbar, guided the ions into the TOF
189 chamber ($\sim 10^{-6}$ mbar) where they were orthogonally extracted and their mass-to-charge ratios determined. The
190 detected signal of each ion is then expressed as counts per second (cps) or counts per second normalized by
191 the sum of reagent (nitrate) ions (norm. cps). More detail about the APi-TOF itself can be found in Junninen
192 et al. (2010). Quantification of HOM remains challenging, and, in this work, we aim at explaining the relative
193 changes of HOM measured at different temperature rather than focusing on their absolute concentration.
194 However, in some instances, we also estimate absolute quantities by applying a calibration factor $C = 1.65 \cdot$
195 10^9 molecules cm^{-3} , (cf. Jokinen et al., 2012, for details on C). This translates to ~ 70 ppt of HOM per
196 normalized counts. As no calibrations were performed during the ACCHA experiments, the value was taken
197 from a sulfuric acid calibration (methodology according to Kürten et al., 2012) performed during an earlier
198 measurement campaign. While associated with a large uncertainty (estimated to be at least -50% / $+100\%$)
199 using this value, we obtained HOM molar yields (as described in later sections) of a similar range as earlier
200 studies (Jokinen et al., 2012; Ehn et al., 2014). We estimated a detection limit from our experimental data at
201 the lowest temperature to be roughly 10^{-5} normalized counts, which correspond to $\sim 10^4$ molecules cm^{-3} .

202

203 **2.5. HOM dynamics in a batch mode chamber**

204 Being configured in batch mode, without active mixing, the AURA chamber is a dynamic reactor where
205 concentrations of products are a function of cumulative sources and cumulative sinks from the start of the
206 experiment. In the case of HOM, their lifetime in the gas phase must be short due to their low vapor pressure
207 and, thus, their fast condensation. This means that the measured HOM concentrations are mainly the result of
208 production and loss having occurred within the previous minutes, as described in more detail in the following
209 section.

210

211 The temporal change in HOM concentrations (i.e. $\frac{d[HOM]}{dt}$) can be expressed as the sum of the production
212 terms and loss terms. The HOM formation is governed by the VOC reaction rate while the loss is dominated
213 by condensation onto particles or walls. For the yield estimation analysis, we focus mainly on the high
214 concentration experiments (i.e. $[\alpha\text{-pinene}] = 50$ ppb), where the high condensation sink (CS, on the order of
215 0.1 s^{-1}) will dominate over the wall loss rate. In a smaller chamber with active mixing, the wall loss rate for
216 low-volatile species has been estimated to be around 10^{-2} s^{-1} (Ehn et al., 2014), and in the AURA chamber we
217 expect it to be much slower, likely on the order of 10^{-3} s^{-1} . Since experiments performed at lower temperatures
218 would reduce the vapor pressure of the resulting oxidized product and form more SOA than in warmer
219 conditions, the variation of the condensation sink was considered in our analysis as we expect higher CS values
220 at lower temperatures.

221

222 Therefore, we can formulate simplified expression as in the following equations:

223

$$\frac{d[HOM]}{dt} = \gamma_{HOM} \cdot k \cdot [VOC] \cdot [O_3] - CS \cdot [HOM] \quad (Eq. 1)$$

225

$$\gamma_{HOM} = \frac{\frac{d[HOM]}{dt} + CS \cdot [HOM]}{k \cdot [VOC] \cdot [O_3]} \quad (Eq. 2)$$

227

228 Herein, γ_{HOM} corresponds to the HOM yield. The temperature-dependent rate constant of α -pinene ozonolysis,
229 k , was taken to be $8.05 \cdot 10^{-16} e^{-640/(273.15+T)} \text{ cm}^3 \text{ molecules}^{-1} \text{ s}^{-1}$, where T is the temperature in degrees Celsius,
230 (Atkinson, 2000; Calvert et al., 2002). Since the majority of HOM are irreversibly lost upon contact with a
231 surface (Ehn et al., 2014), the CS represents the total sink at a time t . The CS was estimated using the measured
232 particle number size distributions from the SMPS (Dal Maso et al., 2005). The molecular properties that govern
233 the CS are the mass accommodation coefficient, the molecular diffusion coefficient and the mean molecular
234 speed. Based on the work by Julin et al. (2014), the mass accommodation coefficient was set to unity. The
235 molecular diffusion coefficient was calculated using Fuller's method (Tang et al., 2015) and the mean

236 molecular speed was calculated using kinetic theory. Both the molecular diffusion and speed depends on
237 molecular composition and on the absolute temperature during the experiments. $C_{10}H_{16}O_7$ was taken as a
238 reference for the CS estimation, being one of the most abundant HOM. In comparison, the CS calculated for
239 the largest molecules (i.e. HOM dimers) were approximately 30 % lower. With the aforementioned
240 assumptions, a distinct yield for each identified HOM of interest can be derived based on Eq. 2, as the slope
241 of a linear fit to the data during an experiment, with $k \cdot [VOC] \cdot [O_3]$ on the x-axis and $\frac{d[HOM]}{dt} + CS \cdot [HOM]$
242 on the y-axis.

243

244

245 **3. Results & Discussion**

246

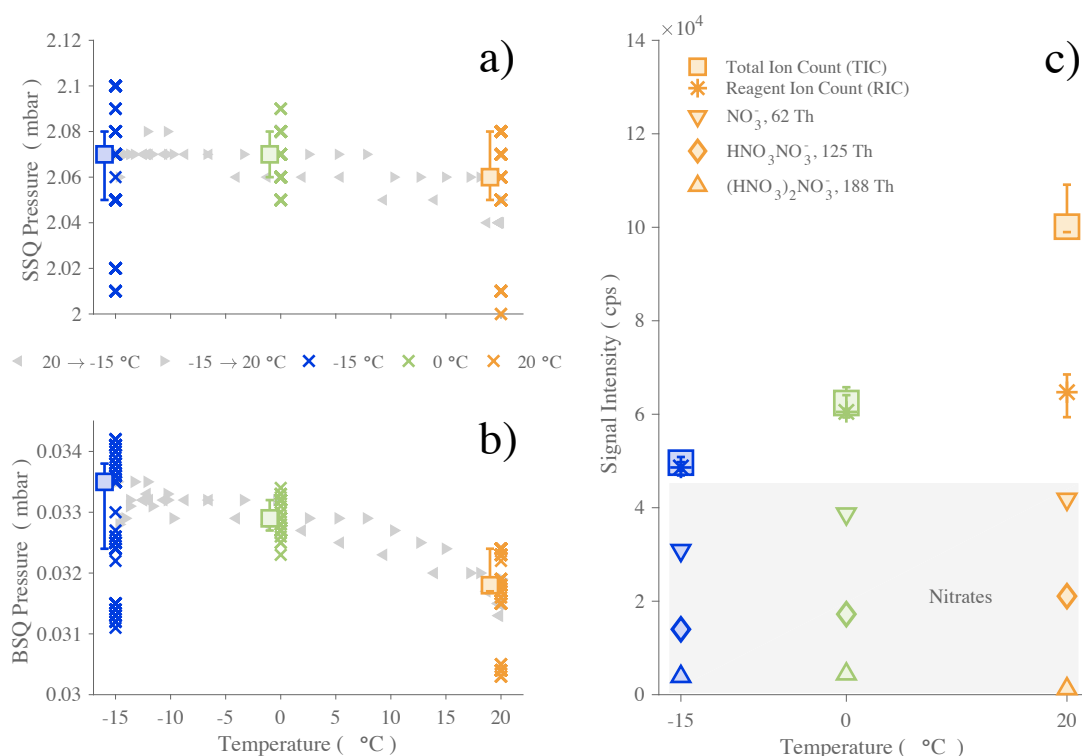
247 **3.1. Effect of the temperature on the CI-APi-TOF**

248 Since this work targets the variation of HOM in relation to temperature, it is necessary to assess the reliability
249 of the CI-APi-TOF measurement towards temperature variations. The sensitivity towards a certain molecule
250 depends to first approximation on the charging efficiency in the CI inlet and the transmission efficiency of the
251 sampled ion in the APi-TOF. The charging efficiency of a HOM is primarily determined by the stability of the
252 $HOM \cdot NO_3^-$ cluster relative to the $HNO_3 \cdot NO_3^-$ cluster (Hyttinen et al., 2015), and we do not expect
253 temperature to cause a large difference in this relative behavior. However, the transmission can be sensitive to
254 small changes, and especially pressures inside the instrument are important to monitor, as the optimal voltages
255 guiding the sampled ions through the instrument have been tuned for specific pressures. The pressures of the
256 two quadrupole chambers (named “SSQ” and “BSQ”, respectively, where the pressure dependence is the
257 largest) as well the Total Ion Count (TIC, i.e. sum of all signals), the Reagent Ion Count (RIC, i.e. sum of
258 nitrate ion signals) and the contributions of each nitrate ion signals are presented in Figure 1. The SSQ
259 pressures (Fig. 1a) were found relatively stable (average: ~ 2.07 mbar) and the BSQ averaged pressure (Fig.
260 1b) was $\sim 3.3 \cdot 10^{-2}$ mbar, which are typical values for this instrument. Unfortunately, the other instrumental
261 pressures (i.e. ion lens assembly chamber or TOF chamber pressures) were not recorded due to sensor failures.
262 However, as these chambers are at low enough pressures that ion-gas collisions are very rare, any possible

263 small variations in the pressures are unlikely to affect our results. When going from the coldest temperature (-
 264 15 °C) to the highest (20 °C), in a continuous temperature ramp, the SSQ pressure decreased by ~0.01 mbar,
 265 corresponding to a relative change of 0.5 % (Fig. 1a). Over the same temperature range, the pressure within
 266 the second chamber (BSQ) decreased by $\sim 1.5 \cdot 10^{-3}$ mbar (~4.5 %) when the temperature varied by 35 °C (Fig.
 267 1a). The same characteristics were observed when comparing across experiments performed at constant
 268 temperatures and for the continuous temperature ramping experiments. The SSQ pressure values below 2.02
 269 mbar at -15 °C and 20 °C, corresponding also to the lowest BSQ pressures measured, were related to
 270 particularly low ambient pressures (~ 981.8 mbar). Thus, the effect of temperature within the AURA chamber
 271 caused smaller variability of the internal pressures than ambient pressure changes.

272

273



274

275 **Figure 1:** Evolution of the CI-API-TOF pressures in the first (a) and second (b) quadrupole chambers (SSQ and BSQ, respectively)
 276 and signal counts (c) as a function of temperature in the AURA chamber. The API pressures (panels a & b) are represented by crosses,
 277 depicting 10-minute averaged data points for all α -pinene ozonolysis experiments, colored by temperature (blue for -15 °C, green for
 278 0 °C and orange for 20 °C). The squares are the median values for each temperature with their 75th and 25th percentiles. Additionally,
 279 the gray triangles relate the data (10-minute averages) of two temperature ramp experiments, from -15 °C to 20 °C (right-pointing

280 triangles) or from 20 °C to -15 °C (left-pointing triangles). Panel c) shows averages of the sum of all ion signals (TIC, square-markers)
281 and the sum of all reagent ion signal (RIC, asterisks-markers). RIC markers also include 25th and 75th percentiles. Nitrate signal
282 contributions are also included separately (markers in gray-shaded area: down pointing triangle for NO_3^- , diamond marker for
283 $\text{HNO}_3\text{NO}_3^-$ and triangle pointing upward for $(\text{HNO}_3)_2\text{NO}_3^-$).

284

285 The RIC signal (Fig. 1c) stayed within the range $5\text{-}7 \cdot 10^4$ cps, with its lowest values observed at -15 °C. The
286 comparatively larger increase in TIC at the highest temperature is mainly explained by the fact that much
287 higher HOM concentrations were formed at 20 °C compared to lower temperature experiments, and the
288 transmission at these masses is generally higher than in the region of the reagent ions (Junninen et al., 2010;
289 Ehn et al., 2011; Heinritzi et al., 2016). We conclude from the above investigations that changes on the order
290 of tens of percent, based on the variation in RIC, occurred in our instrument as the AURA chamber temperature
291 was varied, and that only signal changes larger than this should be attributed to actual perturbations in the
292 chemistry taking place in the chamber.

293

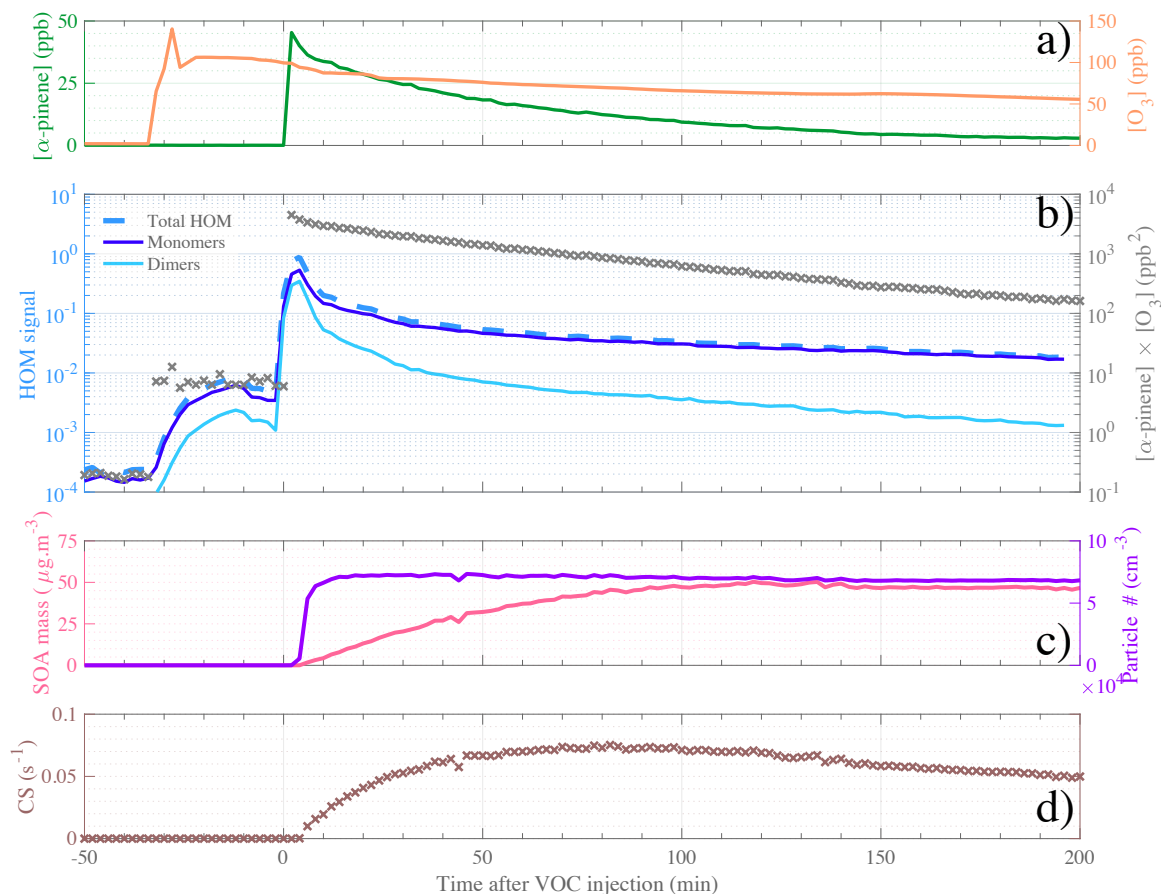
294 **3.2. Ozonolysis reaction in the AURA chamber: a typical α -pinene experiment at 20 °C**

295 Selected gas phase precursors and products, including aerosols, for a high-load (i.e. 50 ppb, during 12-Jan-
296 2017) α -pinene oxidation experiment at 20 °C are shown in Figure 2. The steep increase in α -pinene
297 concentration, measured by PTR-TOF-MS, indicates the start (defined as time 0) of the oxidation reaction
298 experiment (Fig. 2a). The formed aerosol product, i.e. particle number and aerosol mass, are presented in Fig.
299 2c. Herein, we observe an increase of the aerosol mass over the first two hours of the experiment whereas the
300 particle number concentration plateaued in the first ten minutes after VOC injection. On the other hand, the
301 HOM signals (Fig. 2b) show a large increase immediately as the VOC was injected. A smaller increase was
302 also observed when the ozone was introduced, most likely due to residual volatiles reacting with ozone inside
303 the chamber. After the first 10 min, HOM signals start to decrease as the CS (Fig. 2d) rapidly increases under
304 these high aerosol loads. After the first half hour, the CS only changes by some tens of percent, while the
305 VOC oxidation rate (gray crosses in Fig. 2b) decreases around one order of magnitude over the following
306 hours of the experiment. Therefore, concentrations of low-volatile HOM should largely track the decay rate of
307 the VOC oxidation rate, which is also observed. We observe a slower decay of HOM monomers than dimers,

308 suggesting that some of the monomers may be semi-volatile enough to not condense irreversibly upon every
 309 collision with a surface, and/or that the VOC oxidation rate also influences the formation chemistry, as
 310 discussed in more detail in later sections.

311

312

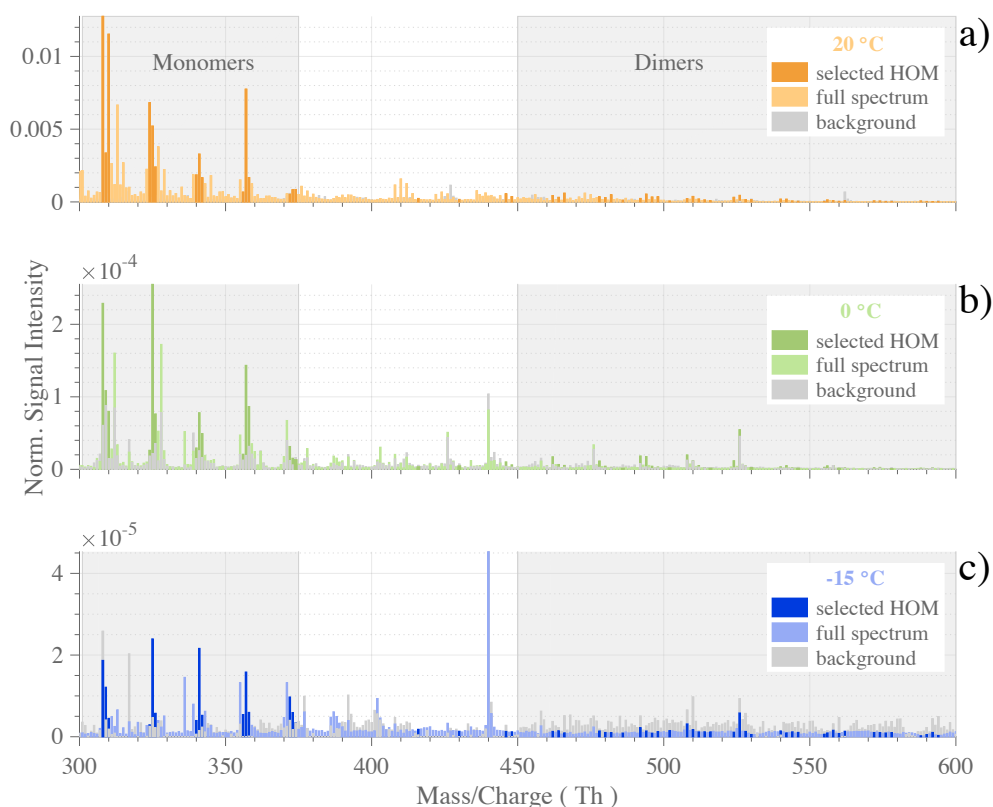


313

314 **Figure 2:** Temporal evolution of the main parameters during a typical α -pinene ozonolysis experiment (initial conditions: $[\alpha\text{-pinene}]$
 315 = 50 ppb, $[\text{O}_3] = 100$ ppb, $T = 20$ °C). Reactant concentrations are shown in Panel a, with α -pinene concentration in dark green and
 316 ozone concentration in orange. HOM signals are plotted in Panel b, with a distinction between Total HOM (dashed medium-blue line),
 317 HOM monomers ($\text{C}_{10}\text{H}_{14-16}\text{O}_{7-11}$, dark blue line) and HOM dimers ($\text{C}_{19-20}\text{H}_{28-32}\text{O}_{10-18}$ light blue line), as well as the product $[\alpha\text{-pinene}]$
 318 $\cdot [\text{O}_3]$ represented by gray cross markers. Panel c depicts the SOA mass (pink line) and the particle concentration (purple line). Panel
 319 d shows the evolution of the condensation sink. The time span (in x-axis) is expressed as minutes after α -pinene injection, thus the
 320 time zero represents the start of the experiment.

321

322 For a more detailed investigation at the HOM formation upon the reaction between ozone and α -pinene, we
323 compare compounds observed in the range between 300 – 600 Thomson (Th) in the CI-APi-TOF, during a
324 background measurement before and from 40 min to 120 min after α -pinene injection for each temperature
325 (Figure 3). The largest HOM signals, highlighted in darker colors, are primarily observed at the highest
326 temperature, but also in the monomer area (300 – 375 Th). The dimer signals (between 450 – 600 Th) are
327 smaller, but still contribute significantly to the total HOM concentration. With the exception of the -15 °C
328 experiment where HOM dimers already reach the background level after 10 min, all molecules selected as
329 representative HOM are present in all the spectra. The detailed peak list of HOM compounds, selected for their
330 high signal intensity, including exact masses and elemental composition is provided in the Appendix (Table
331 A2).



334

335

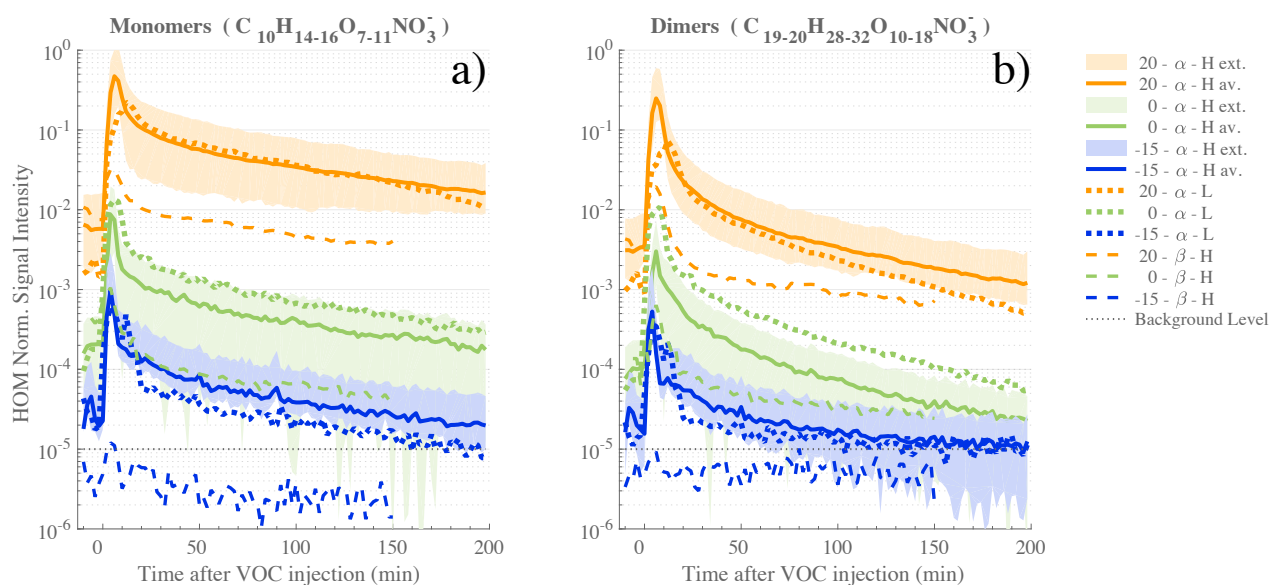
336 **Figure 3:** Typical HOM mass spectra observed during α -pinene ozonolysis experiments (initial conditions: [α -pinene] = 50 ppb, [O₃]
 337 = 100 ppb,) at T = 20 °C (panel a) in orange, T = 0 °C (panel b) in green, T = -15 °C (panel c) in blue. The normalized signals were
 338 averaged over 5 minutes during background measurement before VOC injection (gray bars), and from 40 min to 120 min after α -
 339 pinene injection (colored bars). Specific masses, selected for representing high-intensity HOM, are highlighted in darker colors. Gray-
 340 shaded areas show HOM sub-ranges of monomers and dimers.

341

342 3.3. Effect of the temperature on measured HOM

343 We performed a total of twelve α -pinene ozonolysis experiments with seven at high loading (i.e. [α -pinene] =
 344 50 ppb), out of which two were conducted at 20 °C, two at 0 °C and three at -15 °C. Three experiments were
 345 performed with [α -pinene] = 10 ppb – one for each aforementioned temperature. Experiments with 50 ppb of
 346 β -pinene were also performed at the same three temperatures (see Table A2). An overview of HOM
 347 measurements for the different experiments is shown in Figure 4, with distinction between HOM monomers
 348 (Fig. 4a) and dimers (Fig. 4b) as defined earlier.

349



350

351 **Figure 3:** Time series of HOM measured during the ACCHA campaign. HOM monomer (a) and dimer (b) traces include compounds
 352 with a chemical composition of C₁₀H₁₄₋₁₆O₇₋₁₁ and C₁₉₋₂₀H₂₈₋₃₂O₁₀₋₁₈, respectively. The series are colored based on temperature, orange
 353 for 20 °C experiments, green for 0 °C and blue for -15 °C. Statistics over α -pinene (“ α ” in the legend) high load (50 ppb, “H”)
 354 experiments are shown, with averaged values (“av.” in continuous line) and the maximum and minimum values of the measured HOM

355 signal (bounded shaded area). α -pinene low load (L) experiments are symbolized with colored dotted lines and the β -pinene (“ β ”) experiments by dashed lines. The gray dotted line depicts the estimated background level of the CI-APi-TOF.

357

358 For a similar experiment type (i.e. same initial VOC concentrations), it can be seen that the resulting HOM
359 concentrations were considerably impacted by the temperature at which the oxidation reaction occurred. The
360 signal intensity for HOM monomers from α -pinene measured 30 minutes after the VOC injection was roughly
361 two orders of magnitudes higher at 20 °C compared to 0 °C, and about three orders of magnitude higher
362 compared to the -15 °C experiment. Very similar behavior is observed with respect to temperature for the
363 dimer species as well, but with the differences that (1) less dimers are found in comparison to the HOM
364 monomers and (2) HOM dimer concentrations are found to decrease at a faster rate during the experiment. The
365 faster decrease of dimers compared to monomers results either from a lower production or a higher loss for
366 dimers towards the end of the experiments. We expect that the reduced [α -pinene] and [O_3], leading to slower
367 oxidation rates and consequently lower [RO_2] will have a greater impact on the dimers than the monomers, as
368 the formation rate of dimers is proportional to [RO_2]², while monomers can still be formed efficiently via other
369 RO_2 termination pathways, as discussed earlier.

370

371 When comparing the high (50 ppb) and low (10 ppb) loading α -pinene experiments, HOM signals were within
372 the same range of concentration, and even higher at 0 °C the HOM were even more abundant in the low initial
373 VOC concentration. Although this result may seem surprising at first, it only verifies our assumptions in Eq.
374 1 that the HOM concentration is a relatively simple function of formation and loss rates. Despite the fact that
375 the low-concentration experiments had five times lower [VOC] (and consequently five times lower HOM
376 formation rate), the condensation sink, being the primary loss for HOM, was ~8 times due to reduced aerosol
377 formation. In other words, the loss rates decreased more than the formation rate when the precursor
378 concentration was lowered, resulting in an increase of [HOM].

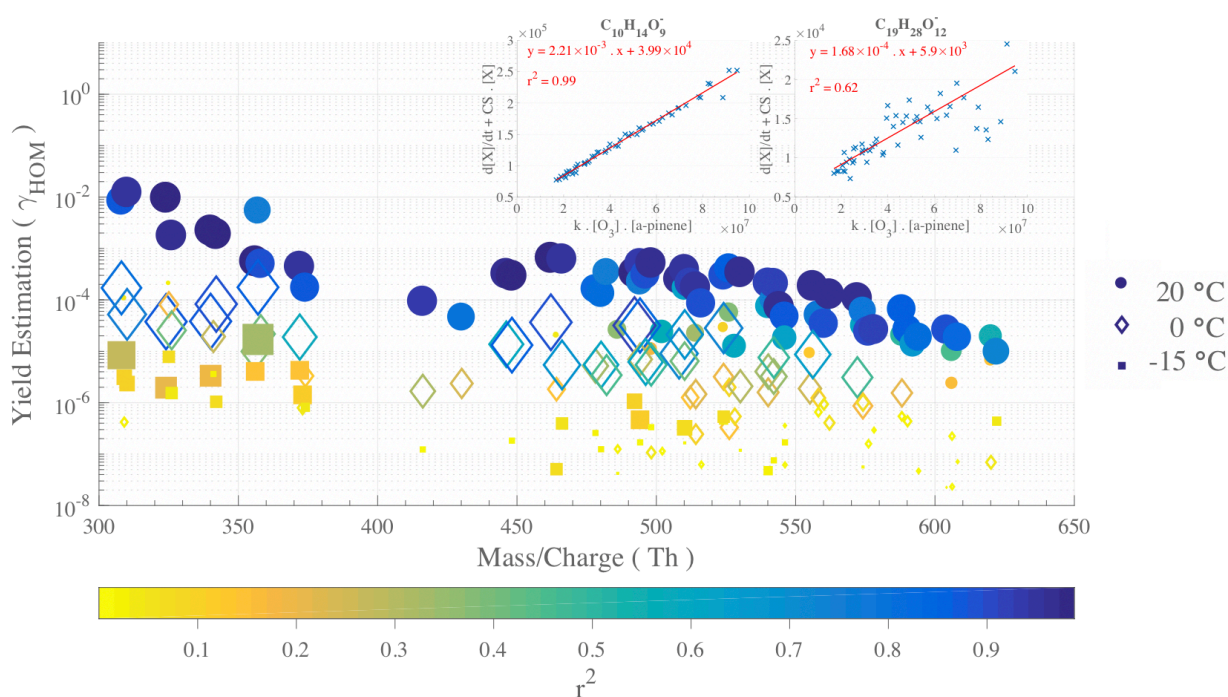
379

380 Finally, the use of β -pinene as HOM precursor produced significantly less HOM, with concentrations being
381 more than a factor of 10 lower compared to experiments performed with α -pinene at the same conditions. This

382 agrees with earlier studies (Jokinen et al., 2014; Ehn et al., 2014) which have shown clearly lower HOM yields
 383 for β -pinene compared to α -pinene ozonolysis. The difference is primarily attributed to the exocyclic double
 384 bond in β -pinene. Note that, the β -pinene HOM concentrations at the lowest temperature, $-15\text{ }^{\circ}\text{C}$, were below
 385 the instrumental limit of detection.

386

387 3.4. Yield estimation and temperature influence for molecule-specific HOM



388

389

390 **Figure 5:** Yield estimations for individual α -pinene HOM from linear fits at $20\text{ }^{\circ}\text{C}$, $0\text{ }^{\circ}\text{C}$ and $-15\text{ }^{\circ}\text{C}$, from 40 to 120 min after α -pinene
 391 injection. Filled circles symbolize data from a $20\text{ }^{\circ}\text{C}$ experiment (12-Jan-2017), diamond symbols illustrate $0\text{ }^{\circ}\text{C}$ data (16-Jan-2017),
 392 and the filled squares represents $-15\text{ }^{\circ}\text{C}$ data (13-Jan-2017). The markers are colored and sized by r^2 values, coefficient of determination,
 393 evaluating the goodness of the linear fit used to derive the yields. The top-right insets show two examples (for $\text{C}_{10}\text{H}_{14}\text{O}_9$ and $\text{C}_{19}\text{H}_{28}\text{O}_{12}$
 394 at $20\text{ }^{\circ}\text{C}$) of the yield determination by robust linear fits to the variables described in the methods section.

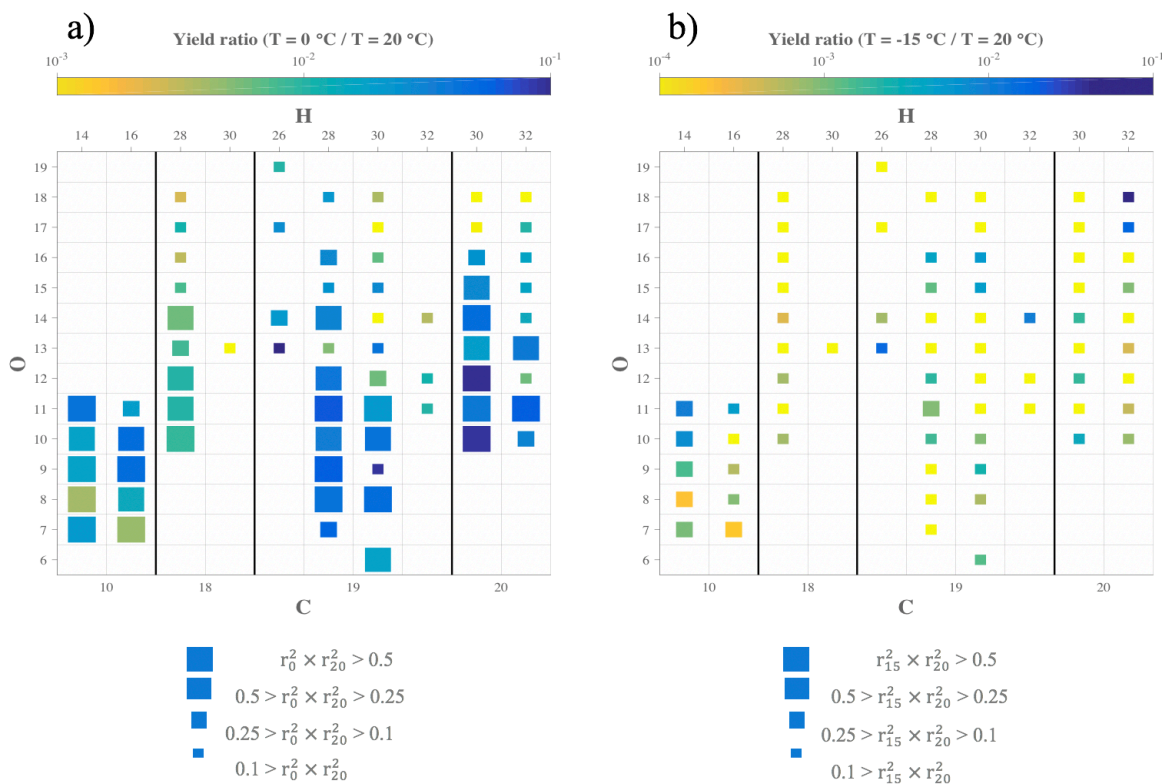
395

396 We determined yield estimates, individually for each HOM of interest, from the results of a robust linear fit as
 397 described in the methods section and Eq. 2, also accounting for the difference in CS between the different
 398 temperatures. In fact, we considered the higher CS for lower temperature experiments. An example of

399 calculated CS, from the measured particle size distribution data, is shown for few experiments in the Appendix
400 (Fig. A1). The yield estimation was performed with a fit with 2-min averaged data points from 40 min to 120
401 min after the VOC injection. These results are shown in Figure 5, with fit examples shown for $C_{10}H_{14}O_9$ and
402 $C_{19}H_{28}O_{12}$ in the insets. As expected, based on Figure 4, the retrieved yield values (γ_{HOM}) decrease
403 considerably with colder reaction conditions, with a total HOM yield (i.e. sum of the individual yields for each
404 temperature) found to be 5.2 % at 20 °C, 0.10 % at 0 °C and $6.3 \cdot 10^{-3}$ % at -15 °C.

405 We again emphasize the large uncertainties in these molar yield estimations, but the HOM yield values for T
406 = 20 °C does agree well with earlier reported values (e.g. Ehn et al. (2014), Jokinen et al. (2014), Sarnela et
407 al. (2018)). As the largest contribution to the HOM yield comes from the least oxidized monomers (e.g. high
408 signal intensity at 308 Th and 310 Th for $C_{10}H_{14}O_7$ and $C_{10}H_{16}O_7$ respectively), the molar yield may be slightly
409 over-estimated, especially at 20 °C, due to the loss rates possibly being lower than assumed if these HOM are
410 not condensing irreversibly onto the aerosol. γ_{HOM} values are on average higher for HOM monomers than for
411 dimers, with the overall shape of the distribution closely resembling the mass spectrum in Figure 3. We
412 performed the same calculation for the experiment were $[\alpha\text{-pinene}] = 10$ ppb and found total HOM-yields in
413 the same range, as the numbers found at 50 ppb, considering our estimated uncertainty: 8.8 % at 20 °C, 0.25
414 % at 0 °C and $5.5 \cdot 10^{-3}$ % at -15 °C. The slightly higher values may indicate that at the higher loadings,
415 bimolecular RO_2 termination reactions are already occurring so fast that autoxidation is hampered. The total
416 HOM yield decrease when going from 20 °C to 0 °C decreased by a factor 50 at the higher loadings, while the
417 corresponding value at lower loadings was 35.

418



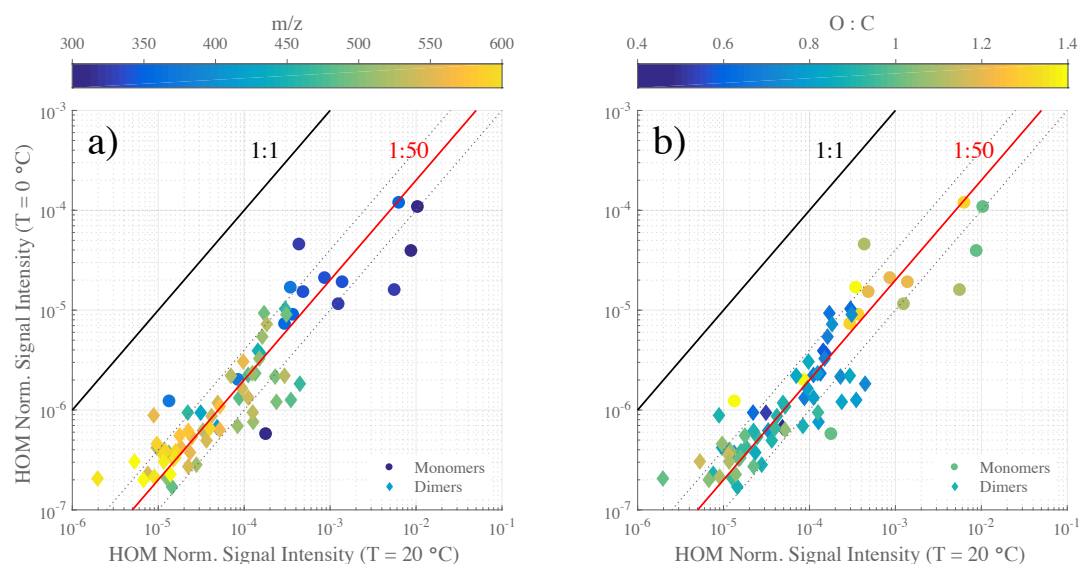
419

420 **Figure 4:** Comparison of yields for specific HOM compositions at different temperatures. Each square symbolizes a specific HOM
 421 measured by the CI-API-TOF. The elemental composition can be read by taking the number of C atoms from the bottom axis, the
 422 number of H atoms from the top axis, and the number of O atoms from the left axis. The size of the square depicts the goodness of fit
 423 (r^2) used to derive the yields, and color shows the ratio of the yield at 0 °C (Panel a) or -15 °C (Panel b) compared to the yield measured
 424 at 20 °C.

425

426 While Figure 5 showed the estimated yields for every HOM at every temperature probed, specific chemical
 427 composition cannot be read from the plot. In order to assess the impact of temperature of the yield of HOM
 428 based on each elemental composition, Figure 6 depicts for each compound the ratio of the yield at 0 °C (Fig.
 429 6a) or -15 °C (Fig. 6b) compared to the yield at 20 °C for a high load experiment of α -pinene ozonolysis. In
 430 Fig. 6a, many larger squares are observable, indicating a good reliability of our comparison analysis, but in
 431 Fig. 6b, it is clear that the HOM concentrations at the lowest temperature were too low to provide much reliable
 432 compound-specific information. From Fig. 6a we see no clear trend in the yield change for any column (i.e.
 433 changing oxygen content HOM with a given amount of C and H). The HOM yields yield ratios between the
 434 two temperatures are primarily within $10^{-2} - 10^{-1}$, meaning that the molecule-specific yields dropped to
 435 between 1-10 % when temperature decreased from 20 °C to 0 °C. If autoxidation of RO_2 decreased this

436 considerably, one could have expected the more oxygenated HOM to decrease more than the less oxygenated
437 ones. However, this did not seem to be the case, as e.g. some of the most abundant HOM $C_{10}H_{14}O_7$, $C_{10}H_{14}O_9$,
438 and $C_{10}H_{14}O_{11}$ seemingly decreased the same amounts.
439



440

441

442 **Figure 7:** Scatter plot on the HOM normalized signal intensity at 0°C and at 20°C. The data points are colored by the mass-to-charge
443 ratio (panel a) or by oxygen-to-carbon ratio (panel b) with distinction between monomer – circle markers - and dimer compounds –
444 diamond markers. Guide lines were added as indicators: 1:1 line – in black, 1:50 line – in red, 1:25 and 1:100 lines - in dotted grey.

445

446 In Figure 7, we show the HOM signal intensities, molecule by molecule based on m/z (Fig. 7a) and on the O:C
447 ratio (Fig. 7b), from the 20 °C-experiment compared to the one at 0 °C. While there is scatter observable
448 between individual HOM, the vast majority of compounds fall close to the 1:50 line, when compared to the
449 distance between the red and the black line. Additionally, the points with the largest scatter (e.g. >50 % from
450 the 1:50-line) show no trends as a function of oxygen content, which also agrees with our observations from
451 Figure 6. One possible interpretation of this is that the rate-limiting step in the autoxidation chain takes place
452 in RO₂ radicals with 6 or less O atoms, which are not detected with our CI-APi-TOF, while the later H-shift
453 reactions are fast enough that other reactions still do not become competitive. These “non-HOM” RO₂ radicals
454 may then also be key molecules for determining the final branching leading to the different observed HOM
455 with 7 or more O atoms. This may shed light on one of the main open challenges (Ehn et al., 2017) in

456 understanding HOM formation, namely how RO₂ radicals with e.g. 6, 8 and 10 O atoms can form within a
457 second, yet the relative distribution of these three does not change if the reaction time is allowed to increase
458 (Berndt et al., 2015). Since the O₁₀-RO₂ (or its closed shell products) are not seen to accumulate over time, our
459 results here provide support for a pathway where the O₆- and O₈-RO₂ are to some extent “terminal” products
460 incapable of further fast H-shift reactions, while the O₁₀-RO₂ has been formed via another branch of the
461 reaction where the autoxidation is able to proceed further. In this branch, the O₆- and O₈-RO₂ are likely only
462 short-lived intermediates. While in no way conclusive, this highlights the need for fast measurements of HOM
463 formation as well as improved techniques for observing less oxidized RO₂ radicals.

464

465 The only compound group where a slight decrease can be seen as a function of O-atom content is the C₂₀H₃₀
466 dimers. Interestingly, these also show some of the smallest yield ratios of all compounds. At the same time,
467 the level of C₁₈ dimers appears to drop most of all compound groups, potentially suggesting that the mechanism
468 through which carbon atoms were lost on the way to the C₁₈ dimers was sensitive to temperature, and at 0 °C
469 the fragmentation was less prominent. It is conceivable that the different branching at 0 °C caused some of the
470 C₁₈ dimer precursors to form C₂₀ dimers instead. However, this issue would need more detailed experiments
471 in order to verify.

472

473 The decrease in HOM yield due to slower RO₂ H-shift rates at lower temperatures was found to be very
474 dramatic under our conditions. However, the exact magnitude of this decrease in HOM yield is determined by
475 the processes competing with the H-shifts. Under our conditions, the RO₂ lifetime is kept quite short, both due
476 to bimolecular (RO₂ + RO₂ or RO₂ + HO₂) reactions and collisions with particles, and therefore any reduction
477 in H-shift rates can strongly reduce the HOM yield. Inversely, under very low loadings, the RO₂ lifetime may
478 be long enough that the temperature decreases from 20 °C to 0 °C may cause much smaller changes in the
479 HOM yields. If the lifetime of RO₂ radicals is clearly longer than the time needed for multiple consecutive H-
480 shifts to take place, HOM yields would decrease only marginally with temperature. In the atmosphere, RO₂
481 lifetime will often be governed by NO, which means that there can exist an intricate dependence of HOM
482 yields as a function of temperature, VOC type, VOC oxidation rate, and NO_x.

483
484

485 **4. Conclusion**

486

487 We present laboratory studies of HOM formation from monoterpene ozonolysis at different temperatures (20
488 °C, 0 °C, and -15 °C). Our main insight is that temperature, in the studied range, considerably impacted the
489 HOM formation, decreasing the observed HOM yield by around 50-fold upon a decrease by 20 °C. The exact
490 temperature dependence of HOM formation in general is likely both VOC- and loading-dependent, due to the
491 competition between autoxidation and termination reactions, and will likely be smaller at lower loadings.
492 While autoxidation is expected to decrease with temperature, our result is still striking as it takes place over a
493 temperature range which is atmospherically relevant for areas where monoterpene emissions are abundant, e.g.
494 the boreal forest. One important observation when decreasing the temperature, was that we found no clear
495 trends of more oxygenated HOM decreasing more than the less oxygenated. This, in turn, suggested that the
496 autoxidation for the species with ~6 oxygen atoms to species with ~10 oxygens was not strongly impacted by
497 the colder temperature in our experiment. This meant that the total HOM yield, as well as the final HOM
498 distribution, were mainly determined by the first H-shift steps, i.e. in the region where the CI-API-TOF is
499 unable to measure. This highlights the need for more comprehensive observations of autoxidation, allowing
500 direct observations of the critical steps determining the HOM yields and, subsequently, the production rate of
501 low-volatile organic compounds able to form secondary organic aerosol.

502

503

504 **Authors Contribution**

505

506 M. Bilde, M. Ehn, and M. Glasius and H. Pedersen supervised the ACCHA campaign. L. Quéléver, M. Ehn,
507 K. Kristensen, and M. Bilde designed the experiments. K. Kristensen and L. N.Jensen initialized the chamber
508 for experiments. L. Quéléver performed the measurement and analyzed the gas-phase HOM. K. Kristensen
509 and L. N. Jensen measured and analyzed the aerosol phase. K. Kristensen, B. Rosati and R. Teiwes measured

510 and analyzed the VOCs and their semi-volatile oxidation production, also supervised by R. Bossi. M. Ehn, K.
511 Daellenbach, O. Peräkylä and P. Roldin guided and helped the analysis of HOM yield performed by L.
512 Quéléver. L. Quéléver prepared the manuscript with the contribution from all co-authors.

513

514

515 **Acknowledgments**

516

517 This work was funded by the European Research Council (Grant n°: 638703-COALA), the Academy of
518 Finland Center of Excellence program (Grant n°: 307331), Aarhus University and the Aarhus University
519 Research Foundation. We also thank Henrik Skov (Aarhus University) for the use of the PTR-TOF-MS. We
520 thank Anders Feilberg (Aarhus University) for assistance in relation to the PTR-TOF-MS. We express our
521 gratitude for the free use of mass spectrometry analysis tools: ToFTools freeware provided by Heikki Junninen
522 (University of Tartu). Otso Peräkylä thanks the Vilho, Yrjö & Kalle Väisälä Foundation. We finally thank
523 Matti Rissanen (Tampere University & University of Helsinki) and Theo Kurtén (University of Helsinki) for
524 their spontaneous input on this work.

525

526

527 **References**

528

529 Atkinson, R., Winer, A., and Pitts Jr, J.: Rate constants for the gas phase reactions of O₃ with the natural
530 hydrocarbons isoprene and α - and β -pinene, Atmospheric Environment (1967), 16, 1017-1020, 1982.

531

532 Atkinson, R.: Atmospheric chemistry of VOCs and NO_x, Atmospheric environment, 34, 2063-2101, 2000.

533

534 Bianchi, F., Kurtén, T., Riva, M., Mohr, C., Rissanen, M. P., Roldin, P., Berndt, T., Crouse, J. D., Wennberg,
535 P. O., and Mentel, T. F.: Highly Oxygenated Organic Molecules (HOM) from Gas-Phase Autoxidation
536 Involving Peroxy Radicals: A Key Contributor to Atmospheric Aerosol, Chemical Reviews, 2019.

537

538 Berndt, T., Richters, S., Kaethner, R., Voigtländer, J., Stratmann, F., Sipilä, M., Kulmala, M., and Herrmann,
539 H.: Gas-phase ozonolysis of cycloalkenes: formation of highly oxidized RO₂ radicals and their reactions with
540 NO, NO₂, SO₂, and other RO₂ radicals, *The Journal of Physical Chemistry A*, 119, 10336-10348, 2015.

541

542 Berndt, T., Richters, S., Jokinen, T., Hyttinen, N., Kurtén, T., Otkjær, R. V., Kjaergaard, H. G., Stratmann, F.,
543 Herrmann, H., and Sipilä, M.: Hydroxyl radical-induced formation of highly oxidized organic compounds,
544 *Nature communications*, 7, 13677, 2016.

545

546 Berndt, T., Scholz, W., Mentler, B., Fischer, L., Herrmann, H., Kulmala, M., and Hansel, A.: Accretion Product
547 Formation from Self-and Cross-Reactions of RO₂ Radicals in the Atmosphere, *Angewandte Chemie*
548 *International Edition*, 57, 3820-3824, 2018.

549

550 Calvert, J. G., Atkinson, R., Becker, K. H., Kamens, R. M., Seinfeld, J. H., Wallington, T. H., and Yarwood,
551 G.: *The mechanisms of atmospheric oxidation of the aromatic hydrocarbons*, Oxford University Press, 2002.
552 Crouse, J. D., Nielsen, L. B., Jørgensen, S., Kjaergaard, H. G., and Wennberg, P. O.: Autoxidation of organic
553 compounds in the atmosphere, *The Journal of Physical Chemistry Letters*, 4, 3513-3520, 2013.

554

555 Dal Maso, M., Kulmala, M., Riipinen, I., Wagner, R., Hussein, T., Aalto, P. P., and Lehtinen, K. E.: Formation
556 and growth of fresh atmospheric aerosols: eight years of aerosol size distribution data from SMEAR II,
557 Hyytiälä, Finland, *Boreal Environment Research*, 10, 323, 2005.

558

559 Donahue, N. M., Kroll, J., Pandis, S. N., and Robinson, A. L.: A two-dimensional volatility basis set–Part 2:
560 Diagnostics of organic-aerosol evolution, *Atmospheric Chemistry and Physics*, 12, 615-634, 2012.

561

562 Donahue, N. M., Ortega, I. K., Chuang, W., Riipinen, I., Riccobono, F., Schobesberger, S., Dommen, J.,
563 Baltensperger, U., Kulmala, M., and Worsnop, D. R.: How do organic vapors contribute to new-particle
564 formation?, *Faraday discussions*, 165, 91-104, 2013.

565

566 Dusek, U., Frank, G., Hildebrandt, L., Curtius, J., Schneider, J., Walter, S., Chand, D., Drewnick, F., Hings,
567 S., and Jung, D.: Size matters more than chemistry for cloud-nucleating ability of aerosol particles, *Science*,
568 312, 1375-1378, 2006.

569

570 Ehn, M., Junninen, H., Petäjä, T., Kurtén, T., Kerminen, V.-M., Schobesberger, S., Manninen, H., Ortega, I.,
571 Vehkamäki, H., and Kulmala, M.: Composition and temporal behavior of ambient ions in the boreal forest,
572 *Atmospheric Chemistry and Physics*, 10, 8513-8530, 2010.

573

574 Ehn, M., Junninen, H., Schobesberger, S., Manninen, H. E., Franchin, A., Sipilä, M., Petäjä, T., Kerminen, V.-
575 M., Tammet, H., and Mirme, A.: An instrumental comparison of mobility and mass measurements of
576 atmospheric small ions, *Aerosol Science and Technology*, 45, 522-532, 2011.

577

578 Ehn, M., Kleist, E., Junninen, H., Petäjä, T., Lönn, G., Schobesberger, S., Maso, M. D., Trimborn, A., Kulmala,
579 M., and Worsnop, D.: Gas phase formation of extremely oxidized pinene reaction products in chamber and
580 ambient air, *Atmospheric chemistry and physics*, 12, 5113-5127, 2012.

581

582 Ehn, M., Thornton, J. A., Kleist, E., Sipilä, M., Junninen, H., Pullinen, I., Springer, M., Rubach, F., Tillmann,
583 R., and Lee, B.: A large source of low-volatility secondary organic aerosol, *Nature*, 506, 476, 2014.

584

585 Ehn, M., Berndt, T., Wildt, J., and Mentel, T.: Highly Oxygenated Molecules from Atmospheric Autoxidation
586 of Hydrocarbons: A Prominent Challenge for Chemical Kinetics Studies, *International Journal of Chemical*
587 *Kinetics*, 49, 821-831, 2017.

588

589 Frege, C., Ortega, I. K., Rissanen, M. P., Praplan, A. P., Steiner, G., Heinritzi, M., Ahonen, L., Amorim, A.,
590 Bernhammer, A.-K., and Bianchi, F.: Influence of temperature on the molecular composition of ions and
591 charged clusters during pure biogenic nucleation, *Atmospheric Chemistry and Physics*, 18, 65-79, 2018.

592

593 Hallquist, M., Wenger, J. C., Baltensperger, U., Rudich, Y., Simpson, D., Claeys, M., Dommen, J., Donahue,
594 N., George, C., and Goldstein, A.: The formation, properties and impact of secondary organic aerosol: current
595 and emerging issues, *Atmospheric chemistry and physics*, 9, 5155-5236, 2009.

596

597 Heinritzi, M., Hansel, A., Simon, M., Steiner, G., Wagner, A. C., Kürten, A., and Curtius, J.: submitter:
598 Characterization of the mass-dependent transmission efficiency of a CIMS, *Atmos. Meas. Tech.*, 9, 1449-
599 1460, 2016.

600

601 Hyttinen, N., Kupiainen-Määttä, O., Rissanen, M. P., Muuronen, M., Ehn, M., and Kurtén, T.: Modeling the
602 charging of highly oxidized cyclohexene ozonolysis products using nitrate-based chemical ionization, *The*
603 *Journal of Physical Chemistry A*, 119, 6339-6345, 2015.

604

605 IPCC: Climate change 2013: the physical science basis. Contribution of the Working Group 1 to the Fifth
606 Assessment Report (AR5) of the Intergovernmental Panel on Climate Change, edited by: Stocker, T. F., Qin,
607 D., Plattner, G., Tignor, M., Allen, S., Boschung, J., Nauels, A., Xia, Y., Bex, V., and Midgley, P. M.,
608 Cambridge University Press, Cambridge (UK), New York (USA), 2013.

609

610 Jayne, J. T., Leard, D. C., Zhang, X., Davidovits, P., Smith, K. A., Kolb, C. E., and Worsnop, D. R.:
611 Development of an aerosol mass spectrometer for size and composition analysis of submicron particles,
612 *Aerosol Science & Technology*, 33, 49-70, 2000.

613

614 Jenkin, M. E., Saunders, S. M., and Pilling, M. J.: The tropospheric degradation of volatile organic compounds:
615 a protocol for mechanism development. *Atmospheric Environment* 31, 81–104, 1997.

616

617 Jenkin, M. E., Young, J. C., and Rickard, A. R.: The MCM v3.3.1 degradation scheme for isoprene. *Atmos.*
618 *Chem. Phys.* 15, 11433–11459, 2015.

619

620 Jimenez, J. L., Canagaratna, M. R., Donahue, N. M., Prevot, A. S., Zhang, Q., Kroll, J. H., DeCarlo, P. F.,
621 Allan, J. D., Coe, H., Ng, N. L., Aiken, A. C., Docherty, K. S., Ulbrich, I. M., Grieshop, A. P., Robinson, A.
622 L., Duplissy, J., Smith, J. D., Wilson, K. R., Lanz, V. A., Hueglin, C., Sun, Y. L., Tian, J., Laaksonen, A.,
623 Raatikainen, T., Rautiainen, J., Vaattovaara, P., Ehn, M., Kulmala, M., Tomlinson, J. M., Collins, D. R.,
624 Cubison, M. J., Dunlea, E. J., Huffman, J. A., Onasch, T. B., Alfarra, M. R., Williams, P. I., Bower, K., Kondo,
625 Y., Schneider, J., Drewnick, F., Borrmann, S., Weimer, S., Demerjian, K., Salcedo, D., Cottrell, L., Griffin,
626 R., Takami, A., Miyoshi, T., Hatakeyama, S., Shimono, A., Sun, J. Y., Zhang, Y. M., Dzepina, K., Kimmel, J.
627 R., Sueper, D., Jayne, J. T., Herndon, S. C., Trimborn, A. M., Williams, L. R., Wood, E. C., Middlebrook, A.
628 M., Kolb, C. E., Baltensperger, U., and Worsnop, D. R.: Evolution of organic aerosols in the atmosphere,
629 *Science*, 326, 2009.

630

631 Jokinen, T., Sipilä, M., Junninen, H., Ehn, M., Lönn, G., Hakala, J., Petäjä, T., Mauldin III, R., Kulmala, M.,
632 and Worsnop, D.: Atmospheric sulphuric acid and neutral cluster measurements using CI-APi-TOF,
633 *Atmospheric Chemistry and Physics*, 12, 4117-4125, 2012.

634

635 Jokinen, T., Sipilä, M., Richters, S., Kerminen, V. M., Paasonen, P., Stratmann, F., Worsnop, D., Kulmala,
636 M., Ehn, M., and Herrmann, H.: Rapid autoxidation forms highly oxidized RO₂ radicals in the atmosphere,
637 *Angewandte Chemie International Edition*, 53, 14596-14600, 2014.

638

639 Jokinen, T., Berndt, T., Makkonen, R., Kerminen, V.-M., Junninen, H., Paasonen, P., Stratmann, F., Herrmann,
640 H., Guenther, A. B., and Worsnop, D. R.: Production of extremely low volatile organic compounds from
641 biogenic emissions: Measured yields and atmospheric implications, *Proceedings of the National Academy of*
642 *Sciences*, 201423977, 2015.

643

644 Jordan, A., Haidacher, S., Hanel, G., Hartungen, E., Märk, L., Seehauser, H., Schottkowsky, R., Sulzer, P.,
645 and Märk, T.: A high resolution and high sensitivity proton-transfer-reaction time-of-flight mass spectrometer
646 (PTR-TOF-MS), *International Journal of Mass Spectrometry*, 286, 122-128, 2009.

647

648 Julin, J., Winkler, P. M., Donahue, N. M., Wagner P. E., and Riipinen, I.: Near-unity mass accommodation
649 coefficient of organic molecules of varying structure. *Environ. Sci. Technol.*, 48(20), 12083-12089, 2014.
650

651 Junninen, H., Ehn, M., Petäjä, T., Luosujärvi, L., Kotiaho, T., Kostianen, R., Rohner, U., Gonin, M., Fuhrer,
652 K., and Kulmala, M.: A high-resolution mass spectrometer to measure atmospheric ion composition,
653 *Atmospheric Measurement Techniques*, 3, 1039-1053, 2010.
654

655 Kristensen, K., Jensen, L., Glasius, M., and Bilde, M.: The effect of sub-zero temperature on the formation
656 and composition of secondary organic aerosol from ozonolysis of alpha-pinene, *Environmental Science:
657 Processes & Impacts*, 19, 1220-1234, 2017.
658

659 Kulmala, M., Kontkanen, J., Junninen, H., Lehtipalo, K., Manninen, H. E., Nieminen, T., Petäjä, T., Sipilä,
660 M., Schobesberger, S., and Rantala, P.: Direct observations of atmospheric aerosol nucleation, *Science*, 339,
661 943-946, 2013.
662

663 Kürten, A., Rondo, L., Ehrhart, S., and Curtius, J.: Calibration of a chemical ionization mass spectrometer for
664 the measurement of gaseous sulfuric acid, *The Journal of Physical Chemistry A*, 116, 6375-6386, 2012.
665

666 Mentel, T. F., Springer, M., Ehn, M., Kleist, E., Pullinen, I., Kurtén, T., Rissanen, M., Wahner, A., and Wildt,
667 J.: Formation of highly oxidized multifunctional compounds: autoxidation of peroxy radicals formed in the
668 ozonolysis of alkenes – deduced from structure–product relationships, *Atmos. Chem. Phys.*, 15, 6745-6765,
669

670 Otkjær, R. V., Jakobsen, H. H., Tram, C. M., and Kjaergaard, H. G.: Calculated Hydrogen Shift Rate Constants
671 in Substituted Alkyl Peroxy Radicals, *The Journal of Physical Chemistry A*, 122, 8665-8673, 2018.
672

673 Praske, E., Otkjær, R. V., Crouse, J. D., Hethcox, J. C., Stoltz, B. M., Kjaergaard, H. G., and Wennberg, P.
674 O.: Atmospheric autoxidation is increasingly important in urban and suburban North America, *Proceedings of
675 the National Academy of Sciences*, 115, 64-69, 2018.

676

677 Rissanen, M. P., Kurtén, T., Sipilä, M., Thornton, J. A., Kangasluoma, J., Sarnela, N., Junninen, H., Jørgensen,
678 S., Schallhart, S., and Kajos, M. K.: The formation of highly oxidized multifunctional products in the
679 ozonolysis of cyclohexene, *Journal of the American Chemical Society*, 136, 15596-15606, 2014.

680

681 Rissanen, M. P., Kurtén, T., Sipilä, M., Thornton, J. A., Kausiala, O., Garmash, O., Kjaergaard, H. G., Petäjä,
682 T., Worsnop, D. R., and Ehn, M.: Effects of chemical complexity on the autoxidation mechanisms of
683 endocyclic alkene ozonolysis products: From methylcyclohexenes toward understanding α -pinene, *The*
684 *Journal of Physical Chemistry A*, 119, 4633-4650, 2015.

685

686 Sarnela, N., Jokinen, T., Duplissy, J., Yan, C., Nieminen, T., Ehn, M., Schobesberger, S., Heinritzi, M.,
687 Ehrhart, S., and Lehtipalo, K.: Measurement–model comparison of stabilized Criegee intermediate and highly
688 oxygenated molecule production in the CLOUD chamber, *Atmospheric Chemistry and Physics*, 18, 2363-
689 2380, 2018.

690

691 Saunders, S. M., Jenkin, M. E., Derwent, R. G., and Pilling, M. J.: Protocol for the development of the master
692 chemical mechanism, MCM v3 (part a): tropospheric degradation of non-aromatic volatile organic
693 compounds. *Atmos. Chem. Phys.*, 3, 161–180, 2003.

694

695 Stolzenburg, D., Fischer, L., Vogel, A. L., Heinritzi, M., Schervish, M., Simon, M., Wagner, A. C., Dada, L.,
696 Ahonen, L. R., and Amorim, A.: Rapid growth of organic aerosol nanoparticles over a wide tropospheric
697 temperature range, *Proceedings of the National Academy of Sciences*, 115, 9122-9127, 2018.

698

699 Tang, M. J., Shiraiwa, M., Pöschl, U., Cox, R. A., and Kalberer, M.: Compilation and evaluation of gas phase
700 diffusion coefficients of reactive trace gases in the atmosphere: Volume 2. Diffusivities of organic compounds,
701 pressure-normalised mean free paths, and average Knudsen numbers for gas uptake calculations. *Atmos.*
702 *Chem. Phys.*, 15, 5585–5598, 2015.

703

704 Tröstl, J., Chuang, W. K., Gordon, H., Heinritzi, M., Yan, C., Molteni, U., Ahlm, L., Frege, C., Bianchi, F.,
705 and Wagner, R.: The role of low-volatility organic compounds in initial particle growth in the atmosphere,
706 Nature, 533, 527, 2016.

707

708 Zhang, Q., Jimenez, J. L., Canagaratna, M., Allan, J., Coe, H., Ulbrich, I., Alfarra, M., Takami, A.,
709 Middlebrook, A., and Sun, Y.: Ubiquity and dominance of oxygenated species in organic aerosols in
710 anthropogenically-influenced Northern Hemisphere midlatitudes, Geophysical Research Letters, 34, 2007.

711

712 Zhao, J., Ortega, J., Chen, M., McMurry, P., and Smith, J.: Dependence of particle nucleation and growth on
713 high molecular weight gas phase products during ozonolysis of α -pinene, Atmospheric Chemistry and Physics,
714 13, 9319-9354, 2013.

715

716

717 **Appendix**

718

719 Table A1 : ACCHA Experiment overview

720

| VOC Concentration (ppb) | [VOC] reacted with O3 * | [VOC] reacted with OH * | Temperature (°C) | Date |
|--|-------------------------|-------------------------|------------------|-----------|
| VOC : α- pinene | | | | |
| 50 | | | 20 | 12-Dec-16 |
| 50 | | | -15 | 13-Dec-16 |
| 50 | | | 0 | 19-Dec-16 |
| 50 | | | -15 | 21-Dec-16 |
| 50 | 30.1 | 15.5 | 20 | 12-Jan-17 |
| 50 | | | -15 | 13-Jan-17 |
| 50 | 30.0 | 16.1 | 0 | 16-Jan-17 |
| 10 | 6.48 | 3.04 | 20 | 02-Dec-16 |
| 10 | | | -15 | 07-Dec-16 |
| 10 | 6.30 | 3.14 | 0 | 08-Dec-16 |
| 10 | | | 20 → -15 | 09-Dec-16 |
| 10 | | | -15 → 20 | 20-Dec-16 |
| VOC : β-pinene | | | | |
| 50 | | | 20 | 03-Jan-17 |
| 50 | | | -15 | 04-Jan-17 |
| 50 | | | 0 | 05-Jan-17 |

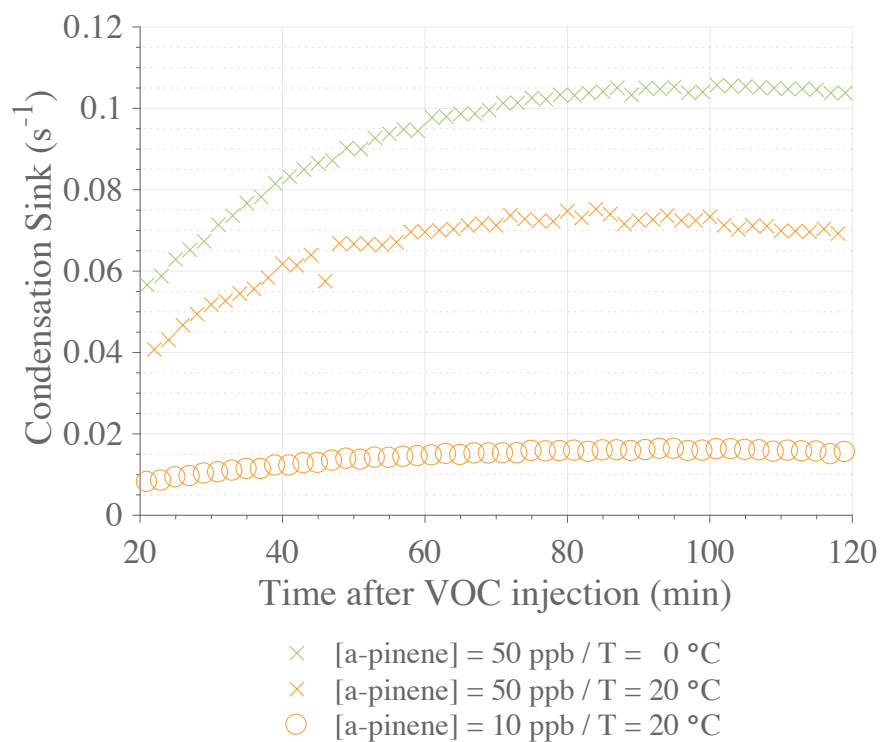
* Estimation based on model simulations using the Master Chemical Mechanism v3.3.2 (Jenkin et al., 1997 & 2015; Saunders et al., 2003)

721

Table A2: Main monoterpene ozonolysis HOM products: Peak list

| Monomers | | Dimers | | | | | |
|---------------|---|---------------|---|---------------|---|---------------|---|
| m/z (Th) | Composition* | m/z (Th) | Composition* | m/z (Th) | Composition* | m/z (Th) | Composition* |
| 308.06 | C ₁₀ H ₁₄ O ₇ | 446.17 | C ₁₉ H ₂₈ O ₈ | 514.14 | C ₁₈ H ₂₈ O ₁₃ | 562.13 | C ₁₈ H ₂₈ O ₁₆ |
| 309.07 | C ₁₀ H ₁₅ O ₇ | 448.18 | C ₁₉ H ₃₀ O ₈ | 514.18 | C ₁₉ H ₃₂ O ₁₂ | 572.15 | C ₂₀ H ₃₀ O ₁₅ |
| 310.08 | C ₁₀ H ₁₆ O ₇ | 462.16 | C ₁₉ H ₂₈ O ₉ | 516.16 | C ₁₈ H ₃₀ O ₁₃ | 574.13 | C ₁₉ H ₂₈ O ₁₆ |
| 324.06 | C ₁₀ H ₁₄ O ₈ | 464.18 | C ₁₉ H ₃₀ O ₉ | 524.13 | C ₁₈ H ₂₆ O ₁₃ | 574.16 | C ₂₀ H ₃₂ O ₁₅ |
| 325.07 | C ₁₀ H ₁₅ O ₈ | 466.16 | C ₁₈ H ₂₈ O ₁₀ | 524.16 | C ₂₀ H ₃₀ O ₁₂ | 576.14 | C ₁₉ H ₃₀ O ₁₆ |
| 326.07 | C ₁₀ H ₁₆ O ₈ | 478.16 | C ₁₉ H ₂₈ O ₁₀ | 526.14 | C ₁₉ H ₂₈ O ₁₃ | 578.12 | C ₁₈ H ₂₈ O ₁₇ |
| 340.05 | C ₁₀ H ₁₄ O ₉ | 480.17 | C ₁₉ H ₃₀ O ₁₀ | 526.18 | C ₂₀ H ₃₂ O ₁₂ | 588.11 | C ₁₉ H ₂₆ O ₁₇ |
| 341.06 | C ₁₀ H ₁₅ O ₉ | 482.15 | C ₁₈ H ₂₈ O ₁₁ | 528.16 | C ₁₉ H ₃₀ O ₁₃ | 588.14 | C ₂₀ H ₃₀ O ₁₆ |
| 342.07 | C ₁₀ H ₁₆ O ₉ | 486.15 | C ₁₇ H ₂₈ O ₁₂ | 530.14 | C ₁₈ H ₂₈ O ₁₄ | 590.16 | C ₂₀ H ₃₂ O ₁₆ |
| 356.05 | C ₁₀ H ₁₄ O ₁₀ | 492.17 | C ₂₀ H ₃₀ O ₁₀ | 540.12 | C ₁₉ H ₂₆ O ₁₄ | 592.14 | C ₁₉ H ₃₀ O ₁₇ |
| 357.05 | C ₁₀ H ₁₅ O ₁₀ | 494.15 | C ₁₉ H ₂₈ O ₁₁ | 540.16 | C ₂₀ H ₃₀ O ₁₃ | 594.12 | C ₁₈ H ₂₈ O ₁₈ |
| 358.06 | C ₁₀ H ₁₆ O ₁₀ | 494.19 | C ₂₀ H ₃₂ O ₁₀ | 542.14 | C ₁₉ H ₂₈ O ₁₄ | 604.14 | C ₂₀ H ₃₀ O ₁₇ |
| 372.04 | C ₁₀ H ₁₄ O ₁₁ | 496.17 | C ₁₉ H ₃₀ O ₁₁ | 542.17 | C ₂₀ H ₃₂ O ₁₃ | 606.12 | C ₁₉ H ₂₈ O ₁₈ |
| 373.05 | C ₁₀ H ₁₅ O ₁₁ | 498.15 | C ₁₈ H ₂₈ O ₁₂ | 544.15 | C ₁₉ H ₃₀ O ₁₄ | 606.15 | C ₂₀ H ₃₂ O ₁₇ |
| 374.06 | C ₁₀ H ₁₆ O ₁₁ | 498.18 | C ₁₉ H ₃₂ O ₁₁ | 546.13 | C ₁₈ H ₂₈ O ₁₅ | 608.13 | C ₁₉ H ₃₀ O ₁₈ |
| | | 502.14 | C ₁₇ H ₂₈ O ₁₃ | 546.17 | C ₁₉ H ₃₂ O ₁₄ | 620.10 | C ₁₉ H ₂₆ O ₁₉ |
| | | 508.17 | C ₂₀ H ₃₀ O ₁₁ | 556.15 | C ₂₀ H ₃₀ O ₁₄ | 620.13 | C ₂₀ H ₃₀ O ₁₈ |
| | | 510.15 | C ₁₉ H ₂₈ O ₁₂ | 558.13 | C ₁₉ H ₂₈ O ₁₅ | 622.15 | C ₂₀ H ₃₂ O ₁₈ |
| | | 510.18 | C ₂₀ H ₃₂ O ₁₁ | 558.17 | C ₂₀ H ₃₂ O ₁₄ | | |
| | | 512.16 | C ₁₉ H ₃₀ O ₁₂ | 560.15 | C ₁₉ H ₃₀ O ₁₅ | | |

* Note that all compounds are detected as cluster with Nitrate Ion (NO₃⁻)



725

726 **Figure A1:** Comparison of the calculated condensation sinks during selected ACCHA runs. Data are shown from 20 min to 120 min
 727 after α -pinene injection for experiments performed at 50 ppb at 0 °C (16-Jan-2017) - green crosses, and 20 °C (12-Jan-2017) – orange
 728 crosses, and at 10 ppb at 20 °C (12-Dec-2016) – orange circles.